

Interfacial viscosity-induced suppression of lateral migration of a surfactant laden droplet in a nonisothermal Poiseuille flow

Devi Prasad Panigrahi ¹, Somnath Santra,¹ Theneyur Narayanaswamy Banuprasad ²,
Sayan Das ³ and Suman Chakraborty^{1,*}

¹*Department of Mechanical Engineering, Indian Institute of Technology Kharagpur,
West Bengal 721302, India*

²*Advanced Technology Development Center, Indian Institute of Technology Kharagpur,
West Bengal 721302, India*

³*Max-Planck Institut für Intelligente Systeme, Heisenbergstr. 3, 70569 Stuttgart, Germany*



(Received 23 September 2020; accepted 12 April 2021; published 21 May 2021)

Understanding and modulating the cross-stream motion of a surfactant-coated droplet in pressure driven flow has great implications in many practical applications. A combination of interfacial viscosity and Marangoni stress acting over a surfactant-coated droplet in pressure driven flow offers greater flexibility to modulate the cross-stream motion of it. Despite the intense theoretical and numerical research towards manipulating the surfactant-laden Newtonian droplets in Poiseuille flow, the experimental investigations are relatively scarce. Herein, we report our study on understanding the influence of interfacial viscosity on the cross-stream motion of a surfactant-coated Newtonian droplet in both isothermal and nonisothermal Poiseuille flow from a theoretical as well as an experimental perspective. A theoretical model has been developed to understand the effect of interfacial viscosity on the lateral migration of a droplet under the assumptions of negligible shape deformation, fluid inertia, and thermal convection. Theoretical analysis is performed under two limiting conditions: (i) when the transport of surfactants is dominated by surface diffusion and (ii) the transportation of surfactants is dominated by surface convection. Our theoretical analysis shows that both the dilatational as well as the shear surface viscosities suppress the lateral migration velocity of the droplet. Experiments have been performed to validate the theoretically predicted droplet trajectories and to understand the influence of channel confinement on the lateral migration of the droplet. Experiments show that the droplet travels faster towards the centerline of the flow in a highly confined domain. The results presented in this study could provide new vistas in designing and analyzing various droplet-based microfluidic, biomedical, and bio-microfluidic devices.

DOI: [10.1103/PhysRevFluids.6.053603](https://doi.org/10.1103/PhysRevFluids.6.053603)

I. INTRODUCTION

In the present era, understanding the interfacial dynamics of droplets appears as an increasingly popular domain of research due to its diverse range of applications in different bio-microfluidic devices [1–3]. Owing to the advancements in the droplet generation technologies, these devices are now making increasing use of droplets for performing tasks such as controlled delivery of drugs, encapsulation of biological cell, analytical detection, etc. [4–8]. The dynamics of droplets is also found to be important in the areas of biomolecules synthesis, mimicking the dynamics of vesicles and single cell analysis [5,9–11]. Knowledge of the motion of droplets in an imposed flow is very

*suman@mech.iitkgp.ac.in

essential for developing an understanding of several naturally occurring processes like the cross-stream motion and positioning of erythrocytes in the microvascular system [12,13]. Control over the motion of droplets and other suspended particles also has implications in flow cytometry and fractionalization of flow field [14,15].

There have been several theoretical and experimental studies on the dynamics of droplets in presence of a background pressure driven flow. Haber and Hetsroni [16] performed an analytical study where they considered a spherical Newtonian droplet in an infinite Poiseuille flow and observed that in the creeping flow limit, the droplet is transported by the flow along the direction of the imposed flow and it does not exhibit any cross-streamwise migration. However, several interesting phenomena can be observed when nonlinear effects such as viscoelasticity [17], Marangoni stress [18], electric stress [19,20], inertia [21], and deformability [22] are considered. One interesting fact is that the migration of a deformable droplet placed in an eccentric position takes place both along the direction of the flow as well as along the cross-streamwise direction [23–26]. For a clean droplet (free of surfactant), the lateral migration is solely influenced by the viscosity ratio of the droplet phase and suspending fluid medium. In a related work, Chan and Leal [27] had performed an analytical study on the migration of a deformable droplet in Stokes' flow and observed that in a two-dimensional Poiseuille flow, the droplet moves away from the flow centerline for the values of viscosity ratio λ (here, λ is the viscosity ratio between the droplet and carrier phase) lying between 0.5 and 1. However, for all other values of λ , it is found that the droplet migrates towards the flow centerline. The existence of inertia [28–30] and viscoelastic nature of the fluid [31,32] are also found to exert significant influence on the cross-stream motion of the droplet. It is interesting to point out that although the Stokes' flow equations obey time-reversal symmetry, the transverse migration of a droplet in parabolic flow does not obey the time-reversal symmetry. For a deformable droplet, this can be attributed to the fact that the droplet experiences a nonuniform distribution of the hydrodynamic traction due to the imposed flow as the strength of the external flow varies along the cross-streamwise direction. This leads to a deformation of the droplet interface, which gives rise to a flow in the surrounding fluid, owing to the no-slip boundary condition on the interface. This deformation-induced flow is responsible for the transverse motion of deformable droplets. In case of spherical droplets coated with surfactants, the origin of the cross-streamwise motion is due to the nonuniform distribution of surfactants. The external flow is responsible for transporting the surfactants across the interface of the droplet, and since the surfactants lower the local interfacial tension, they lead to a nonuniformity in the surface tension. This results in a Marangoni flow across the droplet interface, and due to the no-slip condition induces a flow in the surrounding fluid media. This fluid flow induced by the Marangoni effect is responsible for the transverse migration of a droplet.

The phenomenon of cross-stream migration in parabolic flow is not limited to droplets, it is observed in other soft entities as well, like giant unilamellar vesicles (GUV) and red blood cells (RBC). Danker *et al.* [33] have employed an analytical approach to study the dynamics of GUVs in a Poiseuille flow and have shown that a vesicle always migrates towards the centerline when the viscosity ratio is unity. However, complex migration trajectories such as off-centerline and initial position-dependent migration have been observed for higher values of viscosity ratio between the inner and outer fluids [34]. There have been numerous numerical approaches towards studying the dynamics of vesicles and red blood cells in confined Poiseuille flows [35,36]. Aouane *et al.* [36] have shown that the presence of domain confinement can lead to significant changes in the migration trajectory, it can even lead to a chaotic behavior. In addition to transverse migration, RBCs also exhibit several interesting phenomena like asymmetrical shapes [37] and a transition from tank-treading to tumbling motion [38], depending upon the viscosity ratio and domain confinement. Therefore, the phenomenon of transverse migration of soft entities in microscale pressure-driven flows is universal and the viscosity ratio and domain confinement play key roles in deciding the physical outcome.

It has been shown that the cross-stream motion of droplets in pressure driven flow can be controlled effectively by applying an external temperature gradient [39]. The presence of external

temperature gradient leads to the alteration of temperature distribution on the surface of the droplet. This spatial variation in temperature gives rise to Marangoni stresses along the droplet's interface. The variation of temperature along the flow is found to exert a strong influence on the motion of droplets. From the study of Young *et al.* [40], it has been observed that the solo presence of external temperature gradient can cause the cross-stream motion of the droplet. Following the work of Young *et al.* [40], there have been a number of studies which have focused on understanding thermocapillary motion of droplets in a quiescent medium. The thermocapillary motion of droplets in an imposed Poiseuille flow has been studied analytically by Raja Shekhar and co-workers [41,42]. They have neglected the presence of surfactants and droplet deformation and have shown that under the creeping flow limit, the effect of external temperature gradient and incipient flow can be linearly superimposed.

Surfactants are frequently encountered in various droplet based microfluidic applications. They are either present naturally or are introduced as additives to enhance the stability of emulsions [43]. Along with lowering the interfacial tension, the uneven distribution of surfactants on the interface develops Marangoni stresses [44]. Both the thermal and the surfactant-induced Marangoni stresses have significant influence on the cross-stream motion of droplets [18]. Therefore, a fundamental understanding of the influence of Marangoni stresses on the lateral migration of droplets is of paramount importance. A detailed study related to surfactant-induced cross-stream motion of the droplet is reported in the study by Hanna and Vlahovska [45] and Pak *et al.* [46]. They have performed analytical studies to conclude that the Marangoni stresses developed due to the uneven distribution of surfactants can develop a cross-stream motion of droplets even in the absence of deformation, viscoelasticity, and other nonlinear effects.

Interfacial viscosity refers to the resistance of the interface to deform under the application of stresses. Flumerfelt [47] had characterized the interfacial viscosity of membranes and studied its influence on droplet deformation and orientation. In this study, Flumerfelt has provided a mathematical description of the extra interfacial viscous stresses arising due to the interfacial viscosity. In a related study, Gounley *et al.* [48] studied the effect of interfacial viscosity for the deformation of a droplet in shear flow. They have pointed out that the parameters governing the interfacial viscosity can increase or decrease the tendency of breakup under background shear flow. In the work of Ponce-Torres *et al.* [49], the impact of interfacial viscosity on the breakup of a pendant droplet has been analyzed both theoretically and experimentally. They have reported the accumulation of surfactants in the resulting satellite droplet and have been able to explain it theoretically by incorporating the effect of interfacial viscosity. Recently Das and Chakraborty [50] have performed an analytical and numerical study for investigating the influence of surface viscosity on the axial migration of a droplet in a non-isothermal pressure driven flow. However, the influence of interfacial viscosity on the cross-stream migration of a surfactant-coated droplet in an unbounded nonisothermal Poiseuille flow has not been studied till now.

In our current study, we have developed a theoretical model to elucidate the role of interfacial viscosity on the cross-stream motion of a spherical Newtonian droplet in an unconfined nonisothermal pressure driven flow. For the theoretical analysis, an asymptotic approach is employed in order to tackle the high degree of nonlinearity arising due to the transport of surfactants and the presence of interfacial viscosity. The analysis is performed under two limiting conditions. The first condition is that the transport of surfactant is dictated by surface-diffusion and the other is that the surfactant transport is dictated by the surface-convection mode of transport. Towards studying the effect of interfacial viscosity, two distinct parameters are identified namely: the dilatational Boussinesq number (Bo_d) and the shear Boussinesq number (Bo_s). It has been observed that the dilatational Boussinesq number exerts a stronger influence on droplet motion as compared to the shear Boussinesq number. The magnitude of cross-stream migration velocity of the droplet is found to decrease as both shear as well as dilatational Boussinesq numbers are increased. However, the magnitude of decrease in the lateral velocity of the droplet due to the former is far less as compared to that occurring due to the later. The nature of the decrease in the lateral migration velocity caused due to Bo_s is found to be dependent on the surrounding temperature field. Therefore, it

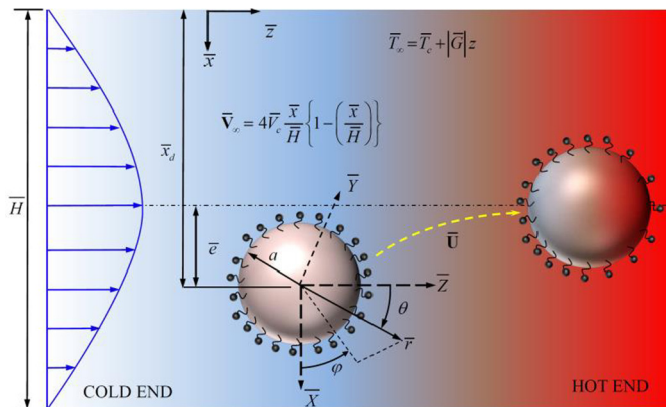


FIG. 1. Schematic representation of a surfactant-coated droplet having radius a suspended in a Plane-Poiseuille flow is shown. There is a linear change of temperature along the flow direction and $|\overline{G}|$ denotes the constant temperature gradient. A spherical co-ordinate system (r, θ, φ) is attached to the center of the droplet. \bar{e} denotes the eccentricity of the droplet and \overline{H} denotes the width of the microchannel. \bar{x}_d symbolizes the distance of the droplet centroid from the wall of the microchannel.

can be concluded that the existence of interfacial viscosity causes the reduction in the cross-stream migration velocity of the droplet and hence, leads to a more naturalistic model for droplet migration in a nonisothermal flow.

The study of confinement-induced hydrodynamics has important implications in the conceptual replication of the scenario prevailing in several microfluidic devices [51–54]. Therefore, experiments are performed to analyze the trajectory of the droplet in a tightly confined domain. These experiments are performed for different degrees of channel confinement. The channel confinement is quantified using a nondimensional ratio called confinement ratio, which is the ratio of the droplet diameter to the width of the channel. Using the experimental results, the effect of channel confinement on the cross-stream migration of the droplet is quantified. The experimental results also match with the theoretical predictions when the confinement ratio is small.

II. THEORETICAL MODEL

A. System description

In the present analysis, we have considered a system, where a spherical droplet of radius a , suspended in another fluid medium is experiencing combined presence of background pressure driven flow and axial temperature gradient (see Fig. 1). The fluids are considered to be Newtonian and incompressible in nature. The properties of fluids are density ρ_i, ρ_e ; viscosity μ_i, μ_e and thermal conductivity k_i, k_e . The subscripts ‘ i ’ and ‘ e ’ denote the droplet phase and ambient fluid phase, respectively. The value of \bar{e} denotes the distance between the droplet centroid and the flow centerline. The value of \bar{e} is determined from $\bar{e} = \bar{x}_d \frac{\overline{H}}{2}$. Here, \bar{x}_d refers to the distance of the droplet centroid from the wall of the microchannel (measured experimentally) and \overline{H} refers to the width of the microchannel. The interface of the droplet is laden by bulk-insoluble surfactants having local concentration $\overline{\Gamma}$. The uniform concentration of surfactants ($\overline{\Gamma}_{eq}$) and the corresponding surface tension at the interface ($\overline{\sigma}_{eq}$) is disturbed due to the imposed fluid flow as well as the nonuniform temperature distribution at the interface (\overline{T}_s). The imposed flow alters the surfactant concentration via the convection mode of surfactant transport across the interface. The temperature field can alter the interfacial tension in two ways: (i) it directly affects the surface tension, and (ii) the thermally induced Marangoni stresses alter the surfactant transport across the interface that also causes a change in the local surface tension. The imposed Poiseuille flow is denoted by \overline{V}_∞ , the

temperature field is denoted by \bar{T}_∞ and the temperature of the cold end is kept constant at \bar{T}_c . All the variables with an over bar denote the dimensional quantities and the ones without it represent the non-dimensional quantities. In the present study, the interfacial viscosity is assumed to remain constant across the interface. The interfacial viscosity is quantified by the values of $Bo_d = \frac{\mu_d}{\mu_e a}$ and $Bo_s = \frac{\mu_s}{\mu_e a}$ which are known as the dilatational and shear Boussinesq number, respectively [50]. These are nondimensional ways of expressing the dilatational and shear viscosities. The dilatational viscosity is the property of an interface due to which it resists expansion and compression. The shear Boussinesq number is physically understood as the resistance of the interface against angular deformation. Therefore, in the theoretical analysis, the effects of Bo_d and Bo_s are investigated on the lateral migration of a droplet in a plane-Poiseuille flow that is acted upon simultaneously by thermal and surfactant induced Marangoni stresses.

B. Assumptions

The important assumptions taken in the theoretical framework are: (i) The effects of fluid inertia are neglected and the pressure and viscous forces govern the flow problem. This implies that the Reynolds number ($Re = \frac{\rho \bar{V}_c a}{\mu_e}$) is very small in magnitude ($Re \ll 1$). Here, \bar{V}_c refers to the velocity at the centerline of the flow. (ii) The convection of thermal energy is considered to be negligible in comparison to diffusion, which results in the thermal Péclet number ($Pe_T = \frac{\bar{V}_c a}{\alpha_e}$) to be negligible. Here, α_e refers to the thermal diffusivity of the suspending fluid. (iii) Natural convection is neglected as both the Grashof number ($Gr = \frac{g \gamma_e \rho_e^2 \Delta T a^3}{\mu_e}$) and the Rayleigh number ($Ra = \frac{g \gamma_e \rho_e \Delta T a^3}{\mu_e \alpha_e}$) are very small ($Gr, Ra \ll 1$). Here, ΔT denotes the characteristic temperature difference. The volumetric expansion coefficient of the ambient fluid is denoted by γ_e . (iv) The shape of the droplet does not deviate from its spherical shape as the interfacial tension is much higher than viscous stresses. Hence, the capillary number $Ca = \frac{\mu_e \bar{V}_c}{\bar{\sigma}_0}$ can be assumed to be very small ($Ca \ll 1$). Here $\bar{\sigma}_0$ refers to the interfacial tension measured at the reference temperature \bar{T}_0 . (v) We have also neglected the effect of wall confinement. (vi) The surfactants are bulk-insoluble and a linear relationship is assumed to hold between the surface tension and the surfactant concentration [55]

$$\bar{\sigma} = \bar{\sigma}_0 - \beta(\bar{T}_s - \bar{T}_0) - R_g \bar{T}_0 \bar{\Gamma}, \quad (1)$$

where \bar{T}_s represent the temperature at the droplet interface and the ideal gas constant is denoted by R_g . β is expressed as $\beta = \frac{-d\bar{\sigma}}{d\bar{T}_g}$. In our experimental study, we have taken a DI water droplet suspended in silicon oil having $\rho_e = 971 \text{ kgm}^{-3}$, $\mu_e = 0.04855 \text{ Nsm}^{-2}$, $\alpha_e = 7 \times 10^{-8} \text{ m}^2\text{s}^{-1}$, and $\gamma_e = 10^{-4}$ [56,57]. The centerline velocity varies in the range of $O(10^{-4}) - O(10^{-5}) \text{ ms}^{-1}$. For surfactant, we have chosen Triton X-100. The obtained nondimensional parameters are: $Re \sim O(10^{-4})$, $Ca \sim O(10^{-4})$, $Pe_T \sim O(10^{-2})$, $Gr \sim O(10^{-6})$, and $Ra \sim O(10^{-2})$. The order of magnitude of nondimensional numbers clearly justifies our assumptions.

C. Nondimensional governing equations and boundary conditions

The nondimensional format adopted in this study is

$$r = \frac{\bar{r}}{a}, \quad \mathbf{u} = \frac{\bar{\mathbf{u}}_c}{\bar{V}_c}, \quad T = \frac{\bar{T} - \bar{T}_0}{|\bar{G}|}, \quad \Gamma = \frac{\bar{\Gamma}}{\Gamma_e q}, \quad \sigma = \frac{\bar{\sigma}}{\bar{\sigma}_0}, \quad p = \frac{\bar{p}}{\mu_e \bar{V}_c a}, \quad \tau = \frac{\bar{\tau}}{\mu_e \bar{V}_c a}. \quad (2)$$

Constant property ratios appearing are $\lambda = \frac{\mu_i}{\mu_e}$ which denotes the viscosity ratio of droplet phase and ambient fluid phase and $\delta = \frac{k_i}{k_e}$ which refers to ratio of thermal conductivity of the droplet phase and the ambient fluid phase. The important nondimensional numbers are: (i) surface Péclet number $Pe_s = \frac{\bar{V}_c a}{D_s}$ (D_s is the surface diffusivity of the surfactant) which signifies the relative strength of the convective mode of surfactant transport to the diffusive mode of surfactant transport along the

interface, (ii) surfactant Marangoni number $Ma_\Gamma = \frac{\Gamma_{eq} R_g T_0}{\mu_e V_c}$ that gives the ratio of the strength of the surfactant-induced nonuniform interfacial tension driven Marangoni convection to the strength of the incipient flow, (iii) thermal Marangoni number $Ma_T = \frac{\beta |\bar{G}|}{\mu_e V_c}$ which is the ratio of the strength of the nonuniform temperature driven Marangoni flow and the imposed Poiseuille flow and (iv) dilatational Boussinesq number $Bo_d = \frac{\mu_d}{\mu_e a}$ which signifies the relative strength of the interfacial dilatational viscous stress with respect to the bulk viscous stress. The shear Boussinesq number is defined as $Bo_s = \frac{\mu_s}{\mu_e a}$, which shows the relative strength of the interfacial shear stress to the bulk viscous stress. In order to theoretically investigate the effects of interfacial viscosity, the magnitude of the dilatational Boussinesq number Bo_d is varied from 0.1 to 10 and the value of the shear Boussinesq number Bo_s is varied from 0.01 to 10. From the experimental data reported in Ponce-Torres *et al.* 2017 [49], it can be inferred that the value of Bo_d and Bo_s can vary from $O(10^{-2})$ to $O(10^3)$. However, we have restricted our results to the above-mentioned ranges in order to depict the most significant variations in the lateral migration velocity because of the presence of interfacial viscosity.

After employing the non-dimensional scheme given in Eq. (2), the following forms of the governing differential equations and related boundary conditions are obtained:

The distribution of temperature is governed by

$$\nabla^2 T_i = 0, \quad (3a)$$

$$\nabla^2 T_e = 0, \quad (3b)$$

subjected to following boundary conditions,

$$\text{as } r \rightarrow \infty, \quad T_e = \zeta r \cos \theta, \quad (4a)$$

$$T_i \text{ is bounded at } r = 0, \quad (4b)$$

$$\text{at } r = 1, \quad T_i = T_e, \quad (4c)$$

$$\text{at } r = 1, \quad \delta(\nabla T_i \hat{n}) = \nabla T_e \hat{n}. \quad (4d)$$

Here, the factor ζ denotes the direction in which temperature gradient is applied and \hat{n} denotes the unit vector normal to the droplet surface. ζ can take binary values, 1 and -1 . The value of $\zeta = 1$ denotes the enhancement of temperature along the flow direction whereas $\zeta = -1$ denotes the reduction of temperature along the flow direction. The distribution of velocity field and pressure field is obtained by solving the following equations:

$$-\nabla p_i + \lambda \nabla^2 \mathbf{u}_i = 0, \quad \nabla \mathbf{u}_i = 0, \quad (5a)$$

$$-\nabla p_e + \nabla^2 \mathbf{u}_e = 0, \quad \nabla \mathbf{u}_e = 0. \quad (5b)$$

The related boundary conditions are read as

$$\text{at } r \rightarrow \infty, \quad (\mathbf{u}_e, p_e) = (\mathbf{V}_e - \mathbf{U}, p_\infty), \quad (6a)$$

$$\mathbf{u}_i \text{ is bounded at } r = 0, \quad (6b)$$

$$\text{at } r = 1, \quad \mathbf{u}_i \mathbf{e}_r = \mathbf{u}_e \mathbf{e}_r = 0, \quad (6c)$$

$$\text{at } r = 1, \quad \mathbf{u}_i = \mathbf{u}_e, \quad (6d)$$

$$\text{at } r = 1, \quad (\boldsymbol{\tau}_e \mathbf{e}_r - \boldsymbol{\tau}_i \mathbf{e}_r)(\mathbf{I} - \mathbf{e}_r \mathbf{e}_r) = Ma_\Gamma (\nabla_s \Gamma) \mathbf{e}_\theta + Ma_T (\nabla_s T) \mathbf{e}_\theta - (\nabla_s \boldsymbol{\tau}_s) \mathbf{e}_\theta. \quad (6e)$$

Based on the Boussinesq-Scriven constitutive law for Newtonian fluids, the surface excess viscous stress can be read as

$$\bar{\boldsymbol{\tau}}_s = 2\mu_s \bar{\mathbf{D}}_s + (\mu_d - \mu_s) \{\mathbf{I}_t : \mathbf{D}_s\} \mathbf{I}_t, \quad (7)$$

where the dilatational and shear viscosities at the droplet interface are denoted by μ_d and μ_s , respectively. The rate of deformation tensor is symbolized by \bar{D}_s and read as

$$\bar{D}_s = \frac{1}{2} \{ \bar{\nabla}_s \bar{\mathbf{u}} \mathbf{I}_t + \mathbf{I}_t (\bar{\nabla}_s \bar{\mathbf{u}})^T \}. \quad (8)$$

After following the non-dimensionalization scheme given in Eq. (2), the following nondimensional form is obtained:

$$\nabla_s \boldsymbol{\tau}_s = (\mathbf{I}_t \nabla) \{ (Bo_d - Bo_s) (\mathbf{I}_t : \nabla) \mathbf{I}_t + 2Bo_s (\mathbf{I}_t \mathbf{D}_s \mathbf{I}_t) \}. \quad (9)$$

Equation (9) represents the general expression for surface excess viscous stresses, by assuming that the values of Bo_d and Bo_s are constant, the following equation is obtained [47]:

$$\nabla_s \boldsymbol{\tau}_s = 2Bo_s \{ (\mathbf{I}_t \nabla) (\mathbf{I}_t \mathbf{D}_s \mathbf{I}_t) \} + (Bo_d - Bo_s) \times \{ \mathbf{I}_t \nabla (\mathbf{I}_t : \nabla \mathbf{u}) + 2\kappa (\mathbf{I}_t : \nabla \mathbf{u}) \}. \quad (10)$$

Here, κ is the mean curvature and $\kappa = -1$ for a spherical droplet.

The surfactant concentration at the interface is governed by the surfactant transport equation, which can be expressed in its nondimensional form as

$$Pe_s \nabla_s (\mathbf{u}_s \Gamma) = \nabla_s^2 \Gamma. \quad (11)$$

Here, \mathbf{u}_s refers to the interfacial fluid velocity of the droplet. In addition to that the surfactant concentration must also satisfy the conservation of mass which is given by

$$\int_{\varphi=0}^{2\pi} \int_{\theta=0}^{\pi} \Gamma(\theta, \varphi) \sin(\theta) d\theta d\varphi = 4\pi. \quad (12)$$

III. ASYMPTOTIC SOLUTION

In this section, we discuss the solution methodology and provide closed-form expressions for the relevant physical variables. The temperature fields both inside and outside the droplet satisfy the homogeneous Laplace equation. Hence, they can be expressed as a linear combination of spherical harmonics [42]:

$$\begin{aligned} T = & \sum_{n=0}^{\infty} \sum_{m=0}^n \{ a_{n,m} r^n \cos(m\varphi) + \hat{a}_{n,m} r^n \sin(m\varphi) \} P_{n,m}(\cos \theta) \\ & + \sum_{n=0}^{\infty} \sum_{m=0}^n \{ b_{-n-1,m} r^{-n-1} \cos(m\varphi) + \hat{b}_{-n-1,m} r^{-n-1} \sin(m\varphi) \} P_{n,m}(\cos \theta), \end{aligned} \quad (13)$$

where $P_{n,m}$ refers to the associated Legendre polynomial. These expressions can be simplified by noting that the temperature inside the droplet is bounded, and the exterior temperature field obeys the far field condition. Mathematically, this translates to the truncation of the negative spherical harmonics for the interior temperature field and positive spherical harmonics for the exterior field. Consequently, the exterior temperature field can be expressed as a linear combination of the far-field temperature and a series of decaying spherical harmonics.

In a similar spirit, the surfactant concentration is also expanded in terms of spherical surface harmonics [46,58], and can be expressed as follows:

$$\Gamma = \sum_{n=0}^{\infty} \sum_{m=0}^n \{ \Gamma_{n,m} \cos(m\varphi) + \Gamma_{n,m} \sin(m\varphi) \} P_{n,m}(\cos \theta). \quad (14)$$

Following [16], we can express the velocity fields using the Lamb's general solution [59], which essentially considers a linear combination of spherical harmonics. Since the velocity field in the

exterior of the droplet satisfies the far-field condition, the higher order harmonics can be truncated, resulting in the following expressions for the velocity and associated pressure fields:

$$\mathbf{u}_e = (\mathbf{V}_\infty - \mathbf{U}) + \sum_{n=1}^{\infty} \nabla \times (\mathbf{r}\chi_{-n-1}) + \nabla \Phi_{-n-1} - \frac{n-2}{2n(2n-1)r^2} \nabla p_{-n-1} + \frac{n+1}{n(2n-1)} \mathbf{r}p_{-n-1}, \quad (15a)$$

$$p_e = p_\infty + \sum_{n=0}^{\infty} p_{-n-1}, \quad (15b)$$

where χ_{-n-1} , p_{-n-1} , and Φ_{-n-1} represent the decaying spherical harmonics. Analogously, the expression for the interior velocity field can be simplified by noting that the velocity field is bounded at the center, which implies that the decaying spherical harmonics should be truncated, resulting in the following expressions for velocity and pressure fields in the interior of the droplet:

$$\mathbf{u}_i = \sum_{n=1}^{\infty} \nabla \times (\mathbf{r}\chi_n) + \nabla \Phi_n + \frac{n+3}{2(n+1)(2n+3)} r^2 \nabla p_n - \frac{n}{(n+1)(2n+3)} \mathbf{r}p_n, \quad (16a)$$

$$p_i = \sum_{n=0}^{\infty} p_n. \quad (16b)$$

Here, χ_n , p_n , and Φ_n denote the growing spherical harmonics.

A. Solution for $Pe_s \ll 1$

From Eqs. (3) and (4), it is evident that the temperature field does not depend on the velocity and interfacial surfactant distribution. Hence, they are solved independently without any regard to the fluid flow and surfactant transport equations. In order to solve the thermal problem, we expand the thermal boundary conditions [Eqs. (4c,d)] using Eq. (13) by setting $r = 1$ and orthogonalize the resulting equations by utilizing the properties of associated Legendre polynomials. This results in a set of equations for each mode, and the resulting solution can be expressed as follows:

$$T_i = \zeta \left(\frac{3}{\delta + 2} \right) r P_{1,0}(\cos(\theta)), \quad (17a)$$

$$T_e = \zeta \left[r + \left(\frac{1-\delta}{2+\delta} \right) \frac{1}{r^2} \right] P_{1,0}(\cos(\theta)). \quad (17b)$$

In order to solve for the combined effects of fluid flow and surfactant transport, a regular perturbation analysis is employed. Any dependent variable Φ is represented by [46]

$$\Phi = \Phi^{(0)} + Pe_s \Phi^{(Pe_s)} + Pe_s^2 \Phi^{(Pe_s^2)} + O(Pe_s^3). \quad (18)$$

The approach used in this study has been successfully applied by [39] to obtain the lateral migration velocity of a droplet suspended in a nonisothermal plane Poiseuille flow. However, in the present study, the focus is on studying the influence of the extra stress terms arising due to interfacial viscosity [Eq. (10)]. The right-hand side (RHS) of Eq. (10) is evaluated by expanding the interfacial velocity as given by Lamb's general solution [Eqs. (15) and (16)]. The contribution of the extra-stress terms due to the presence of interfacial viscosity is manifested in the interfacial force balance. In order to capture this effect, the extra stress term is expressed in terms of the unknown coefficients appearing in the Lamb's solution of the velocity field.

In the low Péclet regime, the surfactant transport equation at any order of perturbation does not depend the velocity field at that order, hence it is solved before the solving the flow field equations.

At the leading order the surfactant concentration is given by

$$\Gamma^{(0)} = 1. \quad (19)$$

In order to obtain the leading order velocity fields, the no-slip [Eq. (6d)], no-penetration [Eq. (6c)] and interfacial force balance [Eq. (6e)] equations have to be expanded using the Lamb's expression of velocity field along with the interfacial temperature and surfactant concentration (at leading order). The resulting equations are orthogonalized leading to a system of linear algebraic equations for the unknown coefficients appearing in the expansion of the velocity field. These coefficients are determined by solving the system of equations and truncating the infinite series of spherical harmonics up to a mode beyond which the magnitude of the coefficients becomes negligibly small.

In the absence of buoyancy forces, the net force on the droplet (\mathbf{F}_H) is a result of the hydrodynamic forces due to pressure and viscous stresses. After obtaining the velocity field, the migration velocity of the droplet at the leading order is obtained using the force-free condition

$$\mathbf{F}_H^{(0)} = 0 \Rightarrow -4\pi \nabla (r^3 p_{-2}^{(0)}) = 0. \quad (20)$$

Here, $\mathbf{F}_H^{(0)}$ refers to the leading order hydrodynamic force that acts on the droplet.

The leading order migration velocity of the droplet is obtained after solving Eq. (20) and can be expressed as

$$\begin{aligned} U_z^{(0)} = & \underbrace{\frac{4(2eH - 2e^2 - \lambda + 3eH\lambda - 3e^2\lambda)}{(2 + 3\lambda)H^2}}_{\text{Effect of imposed flow}} + \underbrace{\frac{2Ma_T\zeta H^2}{(2 + 3\lambda)(\delta + 2)H^2}}_{\text{Effect of temperature gradient}} \\ & - \underbrace{\frac{4Bo_d(3Ma_T\zeta H^2 + 8 + 4\delta)}{3(2 + 3\lambda - 2Bo_d)(\delta + 2)H^2(2 + 3\lambda)}}_{\text{Effect of interfacial viscosity}}, \end{aligned} \quad (21a)$$

$$U_x^{(0)} = U_y^{(0)} = 0 \quad (21b)$$

Here, $U_z^{(0)}$ represents the leading order axial component of the droplet migration velocity, $U_x^{(0)}$ is the leading order lateral migration velocity. It can be concluded from Eq. (21) that the shear surface viscosity does not influence the leading order axial migration of the droplet. The $O(Pe_s)$ surfactant concentration is obtained by substituting the leading order surface velocity into the $O(Pe_s)$ surfactant transport equation. After expanding the surfactant concentration using surface harmonics and solving the linear equations resulting from the orthogonalization of the surfactant transport equation, we observe that only a few components of the infinite sum [Eq. (14)] survive, resulting in the following expression for the $O(Pe_s)$ surfactant concentration:

$$\begin{aligned} \Gamma^{(Pe_s)} = & \Gamma_{1,0}^{(Pe_s)} P_{1,0} \cos(\theta) + \Gamma_{2,1}^{(Pe_s)} P_{2,1} \cos(\theta) \cos(\phi) + \hat{\Gamma}_{2,2}^{(Pe_s)} P_{2,2} \cos(\theta) \sin(2\phi) \\ & + \Gamma_{3,0}^{(Pe_s)} P_{3,0} \cos(\theta) + \Gamma_{3,2}^{(Pe_s)} P_{3,2} \cos(\theta) \cos(2\phi), \end{aligned} \quad (22)$$

where the constant coefficients appearing in Eq. (22) are mentioned in the Supplemental Material [60].

The $O(Pe_s)$ velocity field is obtained by solving the $O(Pe_s)$ governing equations and related boundary conditions. The procedure followed for solving the $O(Pe_s)$ velocity field is similar to the procedure followed while calculating the leading order velocity field, with the exception that the $O(Pe_s)$ surfactant concentration is used in the boundary condition for interfacial force balance. The migration velocity is achieved by solving the force-free condition which is given as follows:

$$\mathbf{F}_H^{(Pe_s)} = -4\pi \nabla (r^3 p_{-2}^{(Pe_s)}) = 0. \quad (23)$$

Here, $\mathbf{F}_H^{(Pe_s)}$ refers to the hydrodynamic force at $O(Pe_s)$.

The $O(Pe_s)$ droplet migration velocity is obtained as follows:

$$U_z^{(Pe_s)} = \frac{2}{9} \frac{Ma_\Gamma (9Ma_\Gamma \zeta H^2 + 24 + 12\delta)}{(2 + 2Bo_d + 3\lambda)(6\lambda + 3\delta\lambda + 4 + 4Bo_d + 2\delta + 2Bo_d\delta)H^2}, \quad (24a)$$

$$U_x^{(Pe_s)} = U_y^{(Pe_s)} = 0. \quad (24b)$$

Finally the $O(Pe_s^2)$ migration velocity is obtained by following a similar procedure and is given by

$$U_z^{(Pe_s^2)} = \frac{2}{9} \frac{Ma_\Gamma^2 (24\lambda + 12\lambda\delta - 9Ma_\Gamma \zeta H^2\lambda)}{\lambda(3\lambda - 2Bo_d + 2)(3\lambda + 2)^2(\delta + 2) - 4Bo_d(2 + 3\lambda - Bo_d)(\delta + 2)H^2}, \quad (25a)$$

$$U_x^{(Pe_s^2)} = \frac{\sum_{i=0}^7 (\sum_{j=0}^7 f_{i,j} Bo_d^j) Bo_s^i}{\Phi(Bo_d, Bo_s, \lambda, \delta)}, \quad (25b)$$

$$U_y^{(Pe_s^2)} = 0. \quad (25c)$$

Finally, the $O(Pe_s^2)$ surfactant concentration is given by

$$\begin{aligned} \Gamma^{(Pe_s^2)} = & \Gamma_{1,0}^{(Pe_s^2)} P_{1,0} \cos(\theta) + \Gamma_{1,1}^{(Pe_s^2)} P_{1,1} \cos(\theta) \cos(\phi) + \Gamma_{2,0}^{(Pe_s^2)} P_{2,0} \cos(\theta) \\ & + \Gamma_{2,1}^{(Pe_s^2)} P_{2,1} \cos(\theta) \cos(\phi) + \Gamma_{2,2}^{(Pe_s^2)} P_{2,2} \cos(\theta) \cos(2\phi) + \hat{\Gamma}_{2,1}^{(Pe_s^2)} P_{2,1} \cos(\theta) \sin(\theta) \\ & + \Gamma_{3,0}^{(Pe_s^2)} P_{3,0} \cos(\theta). \end{aligned} \quad (26)$$

The constant coefficients appearing in Eq. (26) are not mentioned for the sake of brevity. The final form of the lateral migration velocity can be read as

$$U_x = U_x^{(0)} + Pe_s U_x^{(Pe_s)} + Pe_s^2 U_x^{(Pe_s^2)}. \quad (27)$$

To summarize, the surfactant concentration at each order (other than the zeroth order) is coupled to the velocity field of one order lower, via the surfactant transport equation. On the other hand the surfactant and velocity fields of the same order are coupled with each other via the interfacial force balance equation. This results in the occurrence of a cross-stream migration velocity at the $O(Pe^2)$, which bears a strong dependence on the interfacial viscosity.

The temporal variation of transverse position of the droplet is obtained by solving the following linear differential equation:

$$\frac{dx}{dt} = U_x. \quad (28)$$

The final expression is represented in the following form:

$$x = \frac{H}{2} + e^{at} \left(1 - \frac{H}{2}\right), \quad (29)$$

where

$$a = \frac{\sum_{i=0}^4 \sum_{j=0}^{4-i} g_{i,j} Bo_s^j Bo_d^i}{d}. \quad (30)$$

The constants appearing in Eq. (30) are mentioned in the Supplemental Material [60].

B. Solution for $Pe_s \gg 1$

Since the governing equations and related boundary conditions for the thermal problem are independent of the surface Péclet number, therefore the temperature distribution for the high Péclet regime is also given by Eq. (13). Here, the surfactant Marangoni number is assumed to be very large in magnitude, i.e., $Ma_\Gamma \gg 1$ and Ma_Γ^{-1} is taken to be the perturbation parameter for expanding

the dependent variables in the problem [45]. Therefore, all the dependent variables other than the surfactant concentration are expressed in the following form:

$$\chi = \chi^{(0)} + Ma_\Gamma^{-1} \chi^{Ma_\Gamma^{-1}} + O(Ma_\Gamma^{-2}). \quad (31)$$

The surfactant concentration is expressed as

$$\Gamma = 1 + Ma_\Gamma^{-1} \Gamma^{(0)} + Ma_\Gamma^{-2} \Gamma^{(Ma_\Gamma^{-1})} + O(Ma_\Gamma^{-3}). \quad (32)$$

Unlike the case of $Pe_s \ll 1$, here the surfactant and velocity fields of the same order are coupled to each other via the interfacial force balance and surfactant transport equations. Therefore, the surfactant transport equation needs to be solved simultaneously along with the boundary conditions for fluid flow. Other than this, the procedure for obtaining the solution at each order of perturbation remains identical to the case of $Pe_s \ll 1$.

After solving for the flow field, we have utilized the force free condition on the droplet for obtaining the migration velocity of the droplet. The leading order migration velocity of the droplet reads as

$$U_z^{(0)} = \frac{2}{9} \frac{18eH - 18e^2 - 6}{H^2}, \quad (33a)$$

$$U_x^{(0)} = U_y^{(0)} = 0. \quad (33b)$$

The surfactant concentration in leading order can be expressed is in the following form:

$$\begin{aligned} \Gamma^{(0)} = & \Gamma_{1,0}^{(0)} P_{1,0} \cos(\theta) + \Gamma_{2,1}^{(0)} P_{2,1} \cos(\theta) \cos(\phi) + \hat{\Gamma}_{2,2}^{(0)} P_{2,2} \cos(\theta) \sin(2\phi) \\ & + \Gamma_{3,0}^{(0)} P_{3,0} \cos(\theta) + \Gamma_{3,2}^{(0)} P_{3,2} \cos(\theta) \cos(2\phi), \end{aligned} \quad (34)$$

where

$$\begin{aligned} \Gamma_{1,0}^{(0)} = & -\frac{8 + 4\delta + 3Ma_T \zeta H^2}{H^2(\delta + 2)}, \quad \Gamma_{2,1}^{(0)} = \frac{10}{3} \frac{H - 2e}{H^2}, \\ \hat{\Gamma}_{2,2}^{(0)} = & \frac{40}{9} \frac{Bo_s}{H^2(\lambda + 4)}, \quad \Gamma_{3,0}^{(0)} = \frac{7}{3H^2}, \quad \Gamma_{3,2}^{(0)} = -\frac{7}{18H^2}. \end{aligned} \quad (35)$$

The $O(Ma_\Gamma^{-1})$ droplet migration velocity is obtained as

$$U_x^{(Ma_\Gamma^{-1})} = -\frac{2}{3} \frac{4(3\lambda + 2)(\delta + 2) + 9H^2 \zeta Ma_T (\lambda + 4)(H - 2e)}{\lambda + 4(\delta + 2)H^4}, \quad (36a)$$

$$U_z^{(Ma_\Gamma^{-1})} = U_y^{(Ma_\Gamma^{-1})} = 0. \quad (36b)$$

The $O(Ma_\Gamma^{-1})$ surfactant concentration is represented as

$$\begin{aligned} \Gamma^{(Ma_\Gamma^{-1})} = & \Gamma_{1,1}^{(Ma_\Gamma^{-1})} P_{1,1} \cos(\theta) \cos(\phi) + \Gamma_{2,0}^{(Ma_\Gamma^{-1})} P_{2,0} \cos(\theta) + \Gamma_{2,2}^{(Ma_\Gamma^{-1})} P_{2,2} \cos(\theta) \cos(2\phi) \\ & + \Gamma_{3,1}^{(Ma_\Gamma^{-1})} P_{3,1} \cos(\theta) \cos(\phi) + \Gamma_{3,3}^{(Ma_\Gamma^{-1})} P_{3,3} \cos(\theta) \cos(3\phi). \end{aligned} \quad (37)$$

The constant coefficients appearing in Eq. (37) are mentioned in the Supplemental Material [60]. For the sake of brevity, the analytical results are mentioned in a condensed form, however, the MAPLE files containing the analytical solution will be made available upon request.

IV. RESULTS AND DISCUSSIONS

In this section, first we have theoretically established the influence of interfacial viscosity on the lateral migration velocity of a droplet in both isothermal as well as nonisothermal Poiseuille flow. Next, we have performed experiments to justify our theoretical conjectures. Lastly, we have also

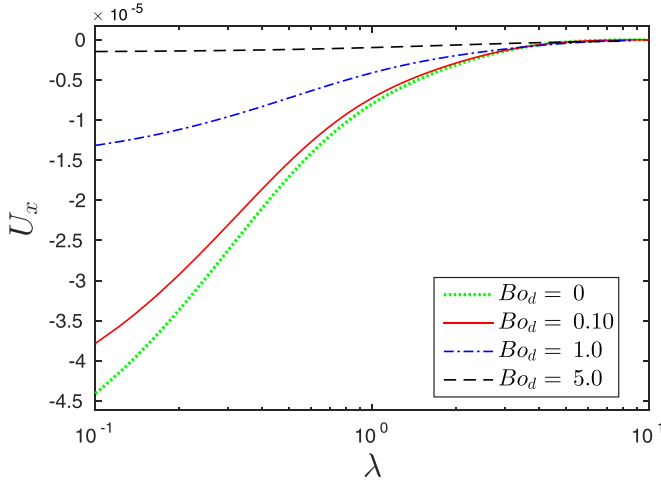


FIG. 2. The variation of U_x is plotted with λ for various values of Bo_d when $Ma_T = 0$, $e = 1$, $Pe_s = 0.1$, $Bo_s = 0$, $H = 10$, $Ma_\Gamma = 0.1$, and $\delta = 0.1$.

illustrated the effect of channel confinement on the trajectory of the droplet under both isothermal and nonisothermal conditions.

A. Effect of interfacial viscosity

1. Isothermal Poiseuille flow

Figure 2 depicts the alteration of the cross-stream migration velocity of the droplet (U_x) with the viscosity ratio of the system (λ) for different dilatational Boussinesq number (Bo_d).

For the present analysis, four different magnitudes of Bo_d have been considered. It can be observed that as the value of Bo_d is increased, the magnitude of U_x decreases. It can be clearly observed that the magnitude of the cross-stream migration velocity is greater for all values of the viscosity ratio when the effect of Bo_d is neglected. Therefore, the presence of dilatational interfacial viscosity actually suppresses the cross-stream migration velocity of the droplet and the magnitude of this suppression increases on increasing the value of the dilatational Boussinesq number. Figure 3 shows the alteration of U_x with λ for different values of the shear Boussinesq number (Bo_s). The magnitude of U_x decreases on increasing the values of Bo_s . However, the magnitude of this decrease is much smaller in comparison to the decrease caused due to the dilatational Boussinesq number.

The physical reason behind the reduction of lateral migration velocity of the droplet due to interfacial viscosity can be identified, if we carefully observe the distribution of surfactant concentration at the droplet interface. Towards this, the contour plots for the surfactant concentration at the interface are plotted in Fig. 4. Figure 4(a) depicts the interfacial surfactant distribution for the case when $Bo_d = 0$ and Fig. 4(b) shows the interfacial surfactant distribution when $Bo_d = 10$. A closer look into Figs. 4(a) and 4(b) reveals that the concentration of surfactant is maximum near the north-west pole and minimum near the north-east pole of the droplet. Therefore, the surfactant distribution for an eccentrically placed droplet is asymmetric both about the transverse as well as about the axial planes. The nonuniformity of surfactant distribution about the transverse plane results in retardation in the axial migration velocity of the droplet. However, the nonuniformity about the axial plane results in the lateral migration of the droplet. Therefore, in the subsequent discussions, more attention will be paid to the non-uniformity in the surfactant concentration about the axial plane. Owing to the closer proximity of the north-pole of the droplet to the centerline of the flow (see Fig. 1), it is exposed to a higher imposed velocity than the south pole. This creates an asymmetry in the surfactant concentration, which in turn creates an asymmetric surface tension

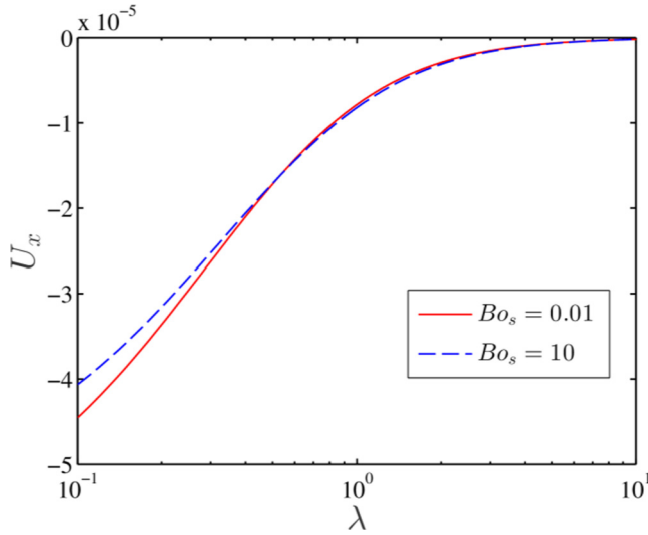


FIG. 3. The variation of U_x is plotted with λ for various values of Bo_s when $Ma_T = 0$, $e = 1$, $Pe_s = 0.1$, $Bo_d = 0$, $H = 10$, $Ma_T = 0.1$, and $\delta = 0.1$.

distribution at the droplet interface. This develops a hydrodynamic force in the cross-streamwise direction that causes the lateral migration of the droplet.

Now we look at the eastern hemispheres of the two droplets shown in Figs. 4(a) and 4(b). Keeping in mind that the primary cause of the lateral migration is the asymmetry in the surfactant concentration, we look into the extent of this asymmetry. A convenient way of representing this is by considering the quantity $(\Gamma_{\max}\Gamma_{\min})$. A larger value of $(\Gamma_{\max}\Gamma_{\min})$ would mean a greater amount of lateral migration of the droplet. On comparison of the extreme values of $\Gamma(\theta, \varphi)$ we find that the value of $(\Gamma_{\max}\Gamma_{\min})$ is lower for the surfactant distribution depicted in Fig. 4(b). Therefore, an increase in the dilatational Boussinesq number results in the decrease in nonuniformity of surfactant distribution at the droplet interface. Consequently, the variations in the surface tension distribution would also be more uniform when the effects of interfacial viscosity are prominent which would lead to a decreased magnitude of the hydrodynamic forces at the droplet interface. Therefore, the

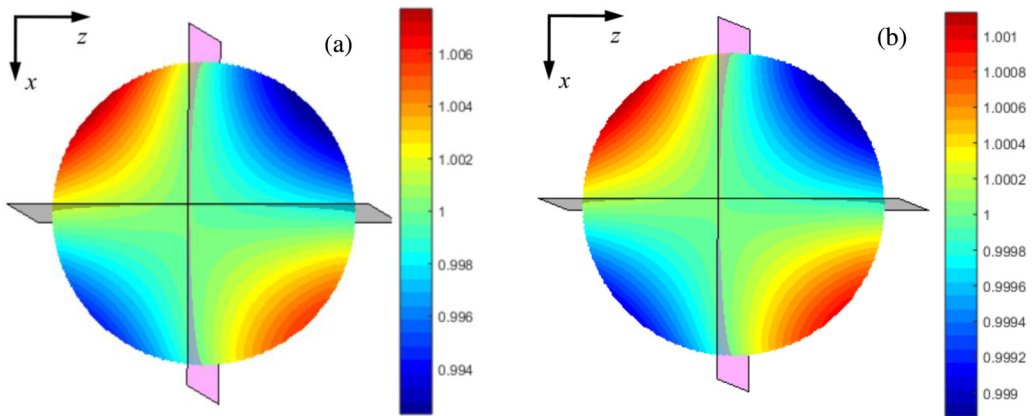


FIG. 4. Surface plot of the surfactant concentration at the droplet interface for (a) $Bo_d = 0$ and (b) $Bo_d = 10$. Other physical parameters are $Pe_s = 0.1$, $Ma_T = 0$, $\delta = 0.1$, $H = 10$, $e = 1$, $Ma_T = 0.1$, $Bo_s = 0$.

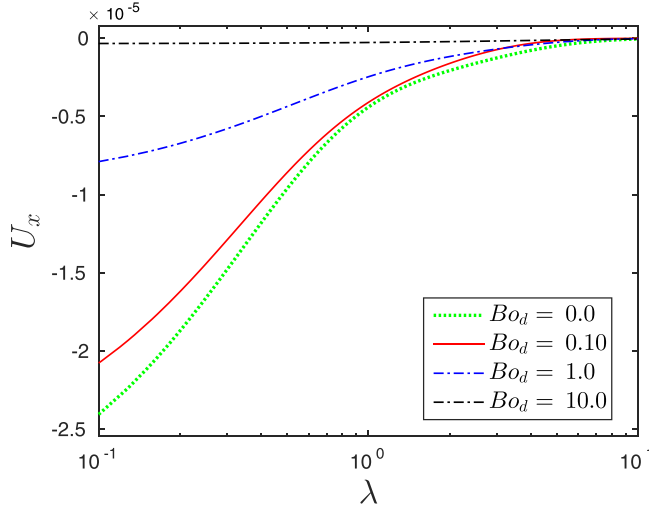


FIG. 5. The variation of U_x is plotted with λ for various values of Bo_d when $Ma_T = 0.10$, $e = 1$, $Pe_s = 0.10$, $Bo_s = 0$, $H = 10$, $Ma_T = 0.10$, $\delta = 0.10$, and $\zeta = 1$.

lateral migration velocity of the droplet would also reduce because of the presence of interfacial viscosity.

In comparing Figs. 2 and 3, we can observe that the decrease in magnitude of the cross-stream migration velocity of the droplet is lesser due to the increase in Bo_s as compared to Bo_d . This can be physically understood by comparing the influence of Bo_d and Bo_s on the surfactant-redistribution. The dilatational surface viscosity quantified using Bo_d , resists the change in local interfacial area, which in turn resists a change in the surface tension, as the surface tension can also be seen as a resistance to increase in surface area of the droplet surface. This limits the extent of the Marangoni stresses which are responsible to distributing the surfactants. On the other hand, the shear surface viscosity affects the surfactant transport by reducing the magnitude of the interfacial velocity. Therefore dilatational viscosity exerts a direct influence on the surfactant distribution by penalizing the variations in surface tension due to changes in the local surface area whereas the shear surface viscosity affects the surfactant transport by damping the interfacial velocity. As discussed in the previous paragraph, variations in surfactant concentration can be directly linked with alterations in the overall migration velocity, this explains why the dilatational viscosity exerts a greater control over the magnitude of the droplet migration velocity.

2. Nonisothermal Poiseuille flow: Temperature gradient applied in the flow direction

Figure 5 depicts the variation in the cross-stream migration velocity of the droplet U_x with λ for different values of the dilatational Boussinesq number Bo_d . It can be observed that the magnitude of U_x is much higher due to the presence of the temperature gradient along the direction of the flow. However, as the value of Bo_d is increased, the magnitude of U_x decreases. In order to explain the decrease in the magnitude of U_x , the distribution of surfactant concentration at the droplet interface is plotted for two different values of the dilatational Boussinesq number.

In the presence of the temperature gradient along the direction of flow, the distribution of the surfactant concentration at droplet interface is shown in Fig. 6. There are several interesting features to note in the contour plots presented in Fig. 6. First, as compared with the contour plots shown in Fig. 4, the lower hemispheres of the droplets in Fig. 6 are inactive as far as exhibiting nonuniformities in surfactant concentration are concerned. This explains a greater magnitude of U_x of the droplets when an external temperature field is applied in the direction of the flow. Now we

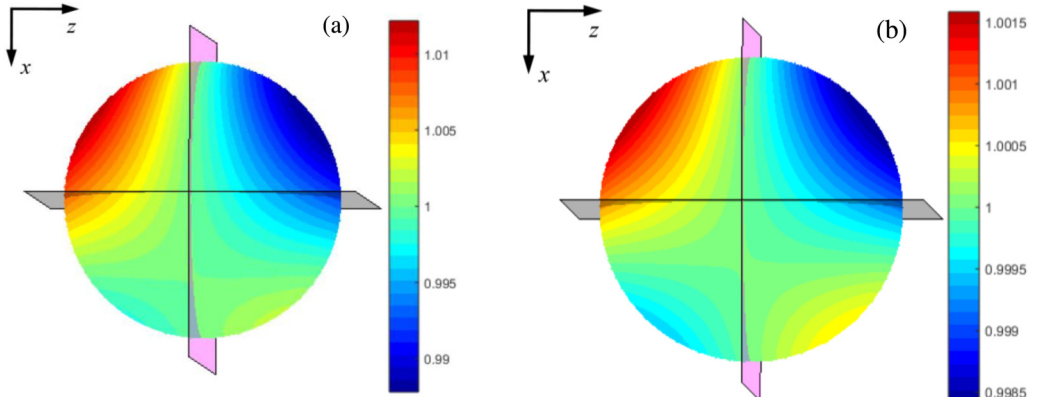


FIG. 6. Surface plot of the surfactant concentration at the droplet interface for (a) $Bo_d = 0$ and (b) $Bo_d = 10$. Other physical parameters are $Pe_s = 0.10$, $Ma_T = 0.1$, $\zeta = 1$, $\delta = 0.10$, $H = 10$, $e = 1$, $Ma_\Gamma = 0.10$, $Bo_s = 0$.

compare Figs. 6(a) and 6(b). In order to provide physical justification to the decrease in magnitude of U_x , we again compare the values of $(\Gamma_{\max}\Gamma_{\min})$ in both the cases. On doing so we conclude that the value of $(\Gamma_{\max}\Gamma_{\min})$ is lower in case (b) and therefore the presence of interfacial viscosity serves to decrease the nonuniformity in the surfactant concentration at the interface which results in a lower magnitude of U_x .

Figure 7 shows the variation in U_x with λ for three different values of the shear Boussinesq number (Bo_s). We observe that as the value of Bo_s is increased from 0.01 to 10, the magnitude of the lateral migration velocity decreases by a noticeable amount. However, as the magnitude of Bo_s is increased further, we do not see any more significant changes in the magnitude of U_x .

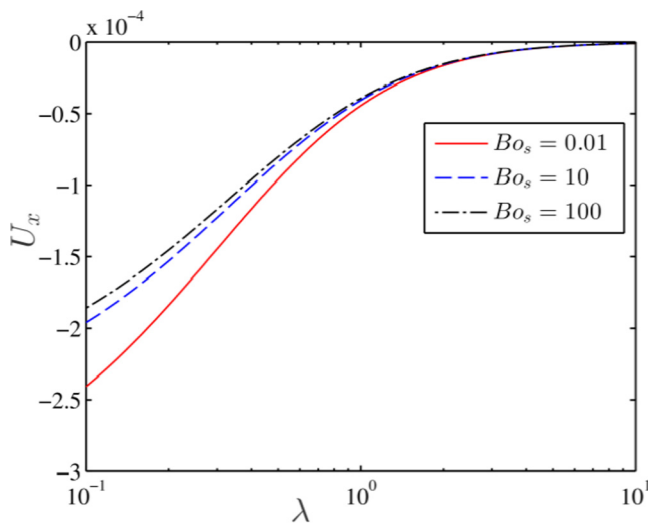


FIG. 7. The variation of U_x is plotted with λ for various values of Bo_s when $Ma_T = 0.1$, $e = 1$, $Pe_s = 0.10$, $Bo_d = 0$, $H = 10$, $Ma_\Gamma = 0.10$, $\zeta = 1$, and $\delta = 0.1$.

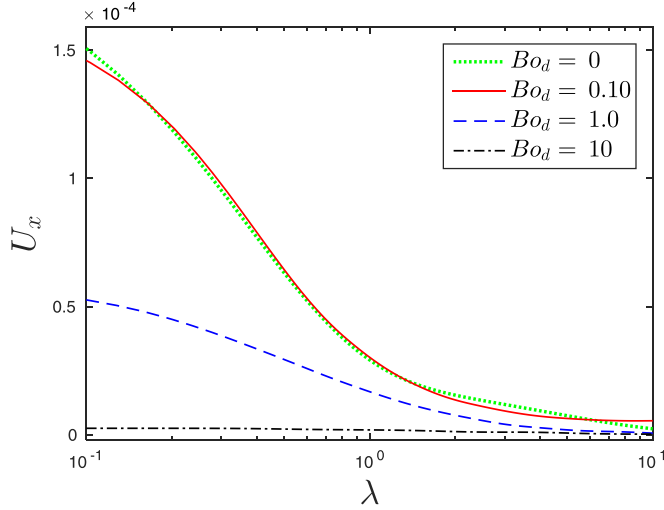


FIG. 8. The variation of U_x is plotted with λ for various values of Bo_d when $Ma_T = 0.1$, $e = 1$, $Pe_s = 0.10$, $Bo_s = 0$, $H = 10$, $Ma_\Gamma = 0.10$, $\zeta = -1$, and $\delta = 0.1$.

3. Nonisothermal Poiseuille flow: Temperature gradient opposite to the flow direction

Now we consider a case where the temperature gradient is applied opposite to the direction of the incipient flow. Towards this, we plot the variation of U_x with λ for different values of the dilatational Boussinesq number Bo_d (see Fig. 8). Firstly, it can be clearly noted that the direction of U_x has reversed. Further, the magnitude of U_x decreases as the value of Bo_d is increased. In order to physically account for this phenomenon, we plot the distribution of surfactant concentration at the interface of the droplet. Figure 9 shows the contour plots for the surfactant concentration at the droplet interface. Here, we see that the surfactant concentration appears to be reversed in comparison to Fig. 6 about the axial plane of the droplet. Due to the presence of a temperature gradient opposite to the direction of the imposed flow, the lower hemisphere of the droplet exhibits a greater non uniformity in the surfactant concentration than the upper hemisphere. Therefore, the droplet migrates in the opposite direction. Now on comparing the magnitudes of $(\Gamma_{\max} - \Gamma_{\min})$ between Figs. 9(a) and 9(b), we find that $(\Gamma_{\max} - \Gamma_{\min})$ is lower in Fig. 9(b). Therefore, the magnitude

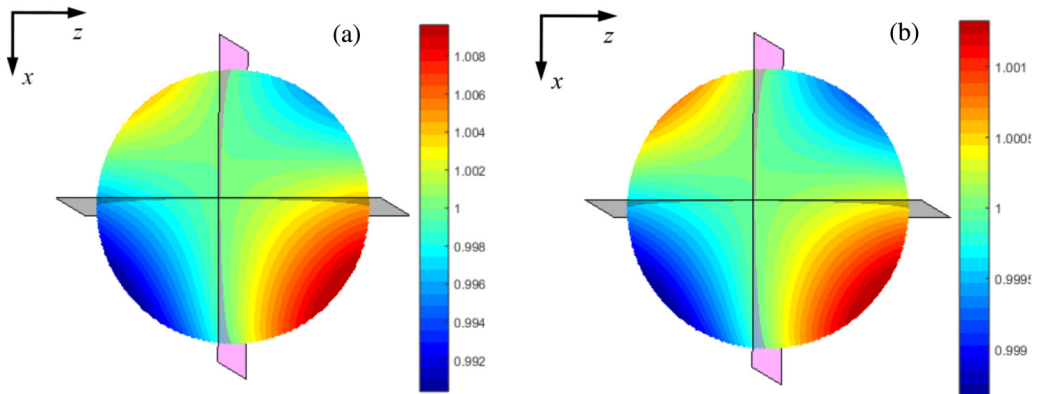


FIG. 9. Surface plot of the surfactant concentration at the droplet interface for (a) $Bo_d = 0$ and (b) $Bo_d = 10$. Other physical parameters are $Pe_s = 0.10$, $Ma_T = 0.1$, $\zeta = -1$, $\delta = 0.10$, $H = 10$, $e = 1$, $Ma_\Gamma = 0.10$, $Bo_s = 0$.

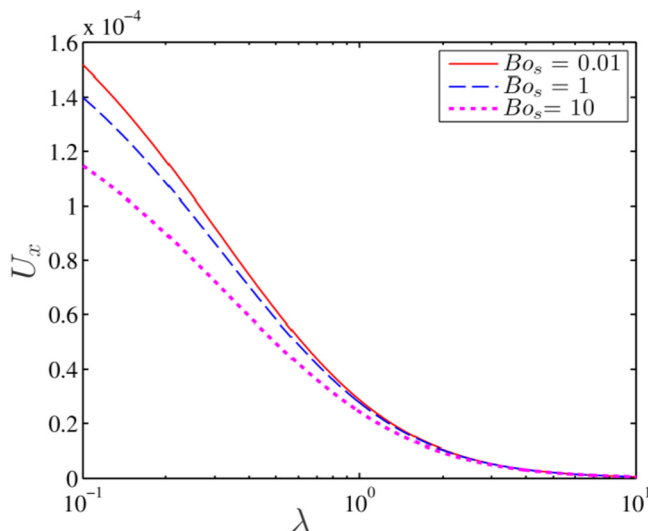


FIG. 10. The lateral migration velocity of the droplet (U_x) is plotted with λ for various values of Bo_s when $Ma_T = 0.1$, $e = 1$, $Pe_s = 0.1$, $Bo_d = 0$, $H = 10$, $\delta = 0.1$, and $\zeta = -1$.

of the cross-stream migration velocity becomes lesser when the value of the dilatational Boussinesq number is increased.

Figure 10 depicts the variation in the lateral migration velocity (U_x) with λ for various values of the shear Boussinesq number (Bo_s). We note that on increasing the value of Bo_s , the magnitude of U_x decreases. However, in this case the decrease is uniform in nature over the values of Bo_s ranging from 0.01 to 10.

B. Experimental investigation

In this section, we depict a comparison of the theoretical findings and results obtained from microfluidic experiments. We show that the present theory, considering the effect of interfacial viscosity provides a much better match, as compared to theoretical results obtained by the negligence of surface viscosity. Further, we also show the effect of domain confinement, which cannot be captured using the present analytical framework. Before discussing the results, we provide a brief overview of the experimental setup and methodology, all the experiments were performed in a controlled ambient condition of 27°C and 50% humidity, the fluids (50 cSt silicon oil and DI water) and chemicals (Triton X-100, nonionic surfactant) used were of analytical grade and used as received.

1. Experimental setup and methodology

To experimentally realize the cross-stream motion of a surfactant-coated droplet in nonisothermal plane-Poiseuille flow as considered in the theoretical analysis, an experimental setup is designed and implemented as depicted in Fig. 11. The setup consists of a PDMS based microfluidic device for droplet generation, an inverted fluorescence microscope (Olympus IX71) coupled with the high-speed camera (Phantom V641) for recording the droplet migration trajectories, a strip heater (tungsten) connected with a voltage source meter (KEITHLEY- 2410) to generate temperature gradient and a temperature measurement system (T-type thermocouple and 3A972A Agilent LXI data acquisition system) to measure the surface temperature.

The PDMS microchannel was fabricated by following a standard microfabrication process involving photolithography followed by soft-lithography [61,62]. The microfluidic device comprises three inlet and one outlet port. Inlet ports are connected to the syringe pumps (Harvard Apparatus PHD 2000: 0-100 ml/min) whereas the outlet port is connected the reservoir through identical

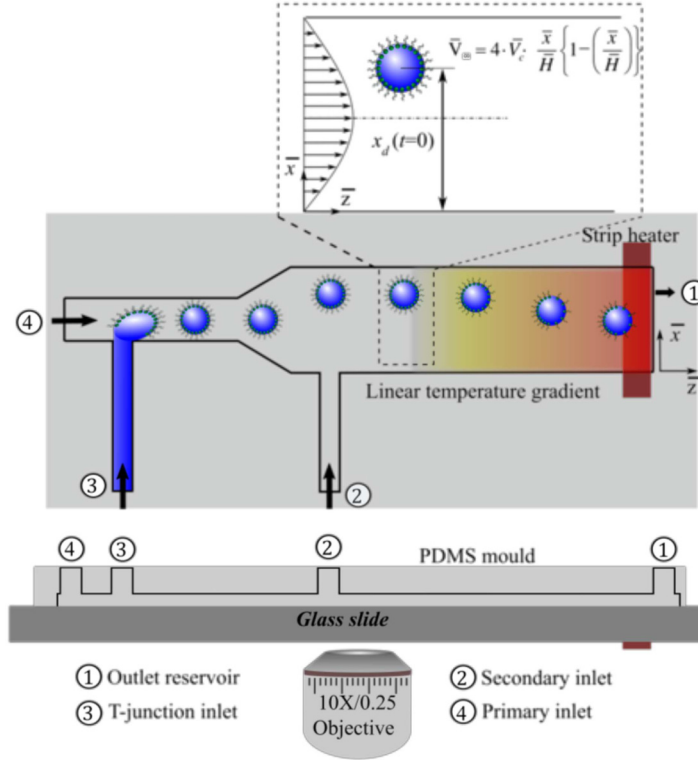


FIG. 11. Schematic representation of the experimental setup developed for the present study. The top portion is the top view of the setup and bottom portion is the side view of the microfluidic device and setup.

Tygon tubes. Inflow of carrier fluid (silicon oil) is created through the primary inlet and the dispersed fluid (a solution of DI water and Triton X-100 having concentration 400 ppm) is pumped through the T-junction inlet. Due to the interplay between the interfacial viscosity and the interfacial tension of continuous fluid and the dispersed fluid at the T-junction, a micrometer droplet is generated as shown in the Fig. 11. As the droplet moves to the wider cross section channel, the droplet is set offset by the inflow of silicon oil through secondary inlet. A nearly linear temperature field is generated along the direction of flow by heating a strip heater by applying the desired voltage. A series of grooves were made in the PDMS device near to wider cross section microchannel, and the thermocouples were inserted into the grooves to measure the temperature. Once the desired temperature gradient attains the steady state, the droplet migration trajectories were captured using the high-speed camera at 200 fps. Experiments were conducted to explore the influence of various confinement ratios. In the experimental analysis, we have also ensured that the depth of the channel does not influence the migration trajectory of the droplet. The detailed procedure followed for arriving at this conclusion is mentioned in the Appendix.

2. Cross-stream motion of the droplet

Figure 12(a) shows a comparison between our experimental observation and theoretical predictions (both with and without considering the effect of interfacial viscosity) on the temporal alteration of transverse position of the droplet centroid subjected to background pressure driven flow and axial temperature gradient. In order to ensure that the data points are free of random fluctuations in the experimental conditions, we have considered the average trajectory obtained from over five distinct experimental runs [63].

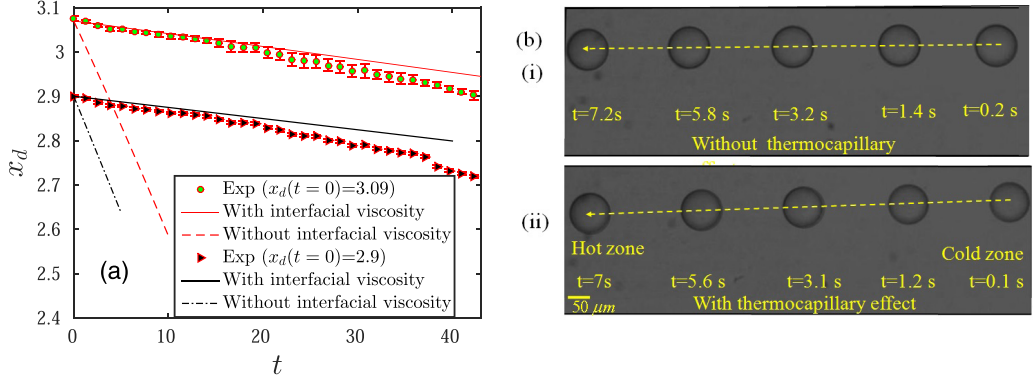


FIG. 12. (a) Comparison of analytical and experimental result on transient variation of the trajectory of droplet centroid under axial temperature gradient at $Wc = 0.25$, (b) experimental images of the droplet at different time frames at $Wc = 0.35$. Other parameters are $Ma_T = 5.5$, $Ma_\Gamma = 3.78$, $Bo_d = 3.28, 2.343, Bo_s = 0.30, 0.2143$ for $Wc = 0.25, 0.35$, respectively, and $Re \sim O(10^{-4})$.

The theoretical trajectory of the droplet without considering the effect of interfacial viscosity is obtained by equating $Bo_d = Bo_s = 0$. From the comparison, it is clearly seen that the present theoretical model considering the effect of interfacial viscosity provides better match with the experimental results and offers a much better approximation to the naturally occurring lateral migration of a droplet laden with bulk-insoluble surfactants and exposed to a nonisothermal Poiseuille flow. In Fig. 12(a), we show the trajectories for two different initial conditions and we observe that the analytically derived trajectory matches with the experiment for both the cases. Hence, we can conclude that the analytical theory works well for different starting positions. However, if the initial position of the droplet is too close to the wall, we would expect the theory to be inaccurate as it does not account for the lift forces due to the walls. The slight deviation of the experimental result from the analytical one (with surface viscosity) is due to the presence of wall in the experimental analysis. In the next paragraph, we have discussed about the impact of channel confinement on the trajectory of the droplet. Figures 12[b(i)] and 12[b(ii)] show the images of the droplet taken at different time intervals. Figure 12[b(i)] shows the droplet's images in an isothermal flow and Fig. 12[b(ii)] depicts the same when temperature gradient acts along the direction of the flow. On comparing the two figures, it is evident that the cross-stream motion of the droplet is more prominent in the second case, i.e., in presence of an applied temperature gradient. Next, we have discussed the effect of the bounding walls on the cross-stream motion of the droplet. In confined domain, the analytical result is unable to predict the trajectory of the droplet accurately. Thus for doing this analysis, we have performed experiment. The effect of the bounding walls is quantified with the help of the domain confinement ratio (Wc), which is defined as the ratio of the droplet size to the width of the channel, i.e., $Wc = 2a/\bar{H}$.

The domain confinement ratio is varied by changing the droplet size by suitably adjusting the flow rate of the carrier fluid phase as explained in the study of Santra *et al.* [61]. Towards studying the influence of the domain confinement on the cross-stream motion of the droplet, the temporal variation of the experimentally measured transverse position of the droplet is plotted for Wc equal to 0.25, 0.30 and 0.35 corresponding to Q_d/Q_c equal to 0.17, 0.22, and 0.33, respectively (see Fig. 13). In order to understand the confluence of domain confinement and thermally induced Marangoni stresses on the droplet in confined domain, two plots are considered: i) the variation of the transverse position of the droplet centroid in an isothermal flow as shown in Fig. 13(a) and ii) the variation of the transverse position of the droplet centroid in a non-isothermal flow as depicted in Fig. 13(b). From these two figures it is noted that the migration of droplet towards channel centerline takes place very rapidly in highly confined domain, i.e., a bigger droplet is found to move faster towards the centerline of the flow than a smaller droplet. Again, by comparing Figs. 13(a) and 13(b) we can

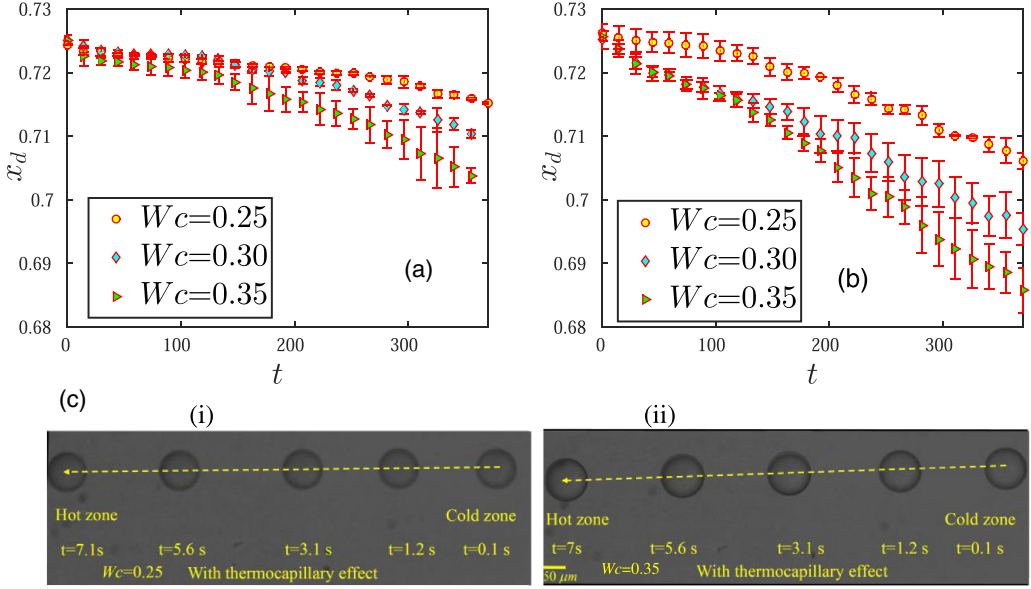


FIG. 13. (a) Temporal evolution of the droplet centroid in an isothermal plane Poiseuille flow. (b) Temporal evolution of droplet centroid in a non-isothermal flow with $Ma_T = 5.5$. (c) Snapshots a single droplet taken at different time intervals when (i) $Wc = 0.25$ and (ii) $Wc = 0.35$. The values of the other parameters are taken as $Ma_T = 3.78$, $Bo_d = 3.28, 2.73, 2.343$, $Bo_s = 0.30, 0.25, 0.2143$ for $Wc = 0.25, 0.30, 0.35$, respectively, and $Re \sim O(10^{-4})$.

also note that due to the presence of the axial temperature gradient, the lateral migration rate of the droplet is further enhanced. Figures 13[c(i)] and 13[c(ii)] show the snapshots of the droplet taken at different time intervals for a domain confinement ratio of 0.25 and 0.35, respectively, where the lateral migration of the droplet is more prominent for the latter case.

For a similar degree of surfactant transport along the interface of the droplet, the magnitude in the difference between the fluid flow velocities in the top and bottom hemispheres is higher for a greater droplet size. Therefore, a larger droplet exhibits a greater asymmetry in the distribution of surfactant along the interface and also results in a more asymmetrical temperature distribution along the interface. This results in a higher value of the Marangoni stresses, therefore resulting in a greater force that moves the droplet towards the flow centerline. Furthermore, the hydrodynamic lift force exerted by the channel wall also causes the faster migration of the droplet towards the centerline and its magnitude enhances with increase in the degree of confinement. Therefore, for a similar value of the axial temperature gradient, the cross-stream migration velocity is higher for a droplet having larger size. It is now known that the presence of an external temperature gradient results in a non-uniform distribution of the temperature along the interface of the droplet. A larger difference in the fluid flow velocities in the two hemispheres results in a larger asymmetry in the temperature distribution along the interface, which leads to a greater value of the thermally induced Marangoni stress along the interface of the droplet. Therefore, the increase in the lateral migration velocity of the droplet due to externally applied temperature gradient is much higher for a larger droplet as compared to a smaller droplet.

V. CONCLUSIONS

In the current analysis, a theoretical model is developed in order to investigate the influence of interfacial viscosity on the lateral migration of a surfactant-coated Newtonian droplet suspended in

a nonisothermal pressure driven flow. Neglecting the effects of fluid inertia, shape deformation and thermal convection, we have obtained analytical expressions for the lateral migration velocity of the droplet for two limiting cases, namely: i) $Pe_s \ll 1$, which corresponds to the diffusion dominated transport of surfactants and ii) $Pe_s \gg 1$, which corresponds to the convection dominated surfactant transport. The first scenario is more relevant from an experimental and application perspective and therefore discussed in detail. In addition to that, we have also performed experiments in order to validate our theoretical findings and studied the effect of channel confinement on the lateral migration of the droplet. After analyzing all the important parameters involved in the physical problem, the following conclusions are made:

(i) The analytical solution considering the effect of interfacial viscosity shows a good agreement with the experimental result on lateral migration of a surfactant-coated droplet in a nonisothermal Poiseuille flow, hence provides a much greater approximation to the naturally occurring lateral migration of the droplet under same condition. Another important fact is that for identical values of the channel width and identical thermal condition, a larger droplet migrates faster towards the centerline of the flow as compared to a smaller one.

(ii) It has been found that the dilatational surface viscosity suppresses the lateral migration of the droplet to a large extent. The effect of dilatational interfacial viscosity has been investigated for three different situations namely i) isothermal flow, ii) nonisothermal flow where the temperature gradient is along the direction of the flow, and iii) nonisothermal flow having a uniform temperature gradient acting in a direction opposite to the incipient flow. In all the three cases, increase in the value of the dilatational Boussinesq number (Bo_d) results in decrease in the magnitude of the lateral migration velocity.

(iii) The shear surface viscosity arises also suppresses the lateral migration velocity of the droplet. Nevertheless, the decrease in the magnitude of lateral migration velocity due to shear surface viscosity is lesser as compared to the decrease occurring due to dilatational surface viscosity. Further, the nature of the decrease in the migration velocity due to shear viscosity is found to have a dependency on thermal environment of the imposed flow. It has also been noted that the decrease in the migration velocity due to shear surface viscosity is more gradual in presence of a uniform temperature gradient opposite to the direction of the flow as compared to an isothermal flow or a uniform temperature field along the flow direction.

ACKNOWLEDGMENTS

S.C. acknowledges support as a Sir J.C. Bose National Fellow, from the Department of Science and Technology, Government of India.

APPENDIX: INVARIANCE OF MIGRATION TRAJECTORY WITH CHANNEL DEPTH

Here, we discuss the experimental validation for negligence of the effect of depth of the microchannel, on the migration trajectory of the droplet. We consider two microchannels, one having a depth of $366 \mu\text{m}$ (microchannel 1) and another having a depth of $442 \mu\text{m}$ (microchannel 2). The depths of the two channels were measured using the Dektat 150 surface profiler and the results are depicted in Fig. 14(a). Next, we compared the migration trajectory of a droplet having diameter $\sim 100 \mu\text{m}$, in both the channels and depicted the same in Fig. 14(b). The comparison shows that the two trajectories are nearly overlapping each other, with very minor differences. The depth of the droplet within the channel is set as a result of the confluence between the lift forces from the walls and buoyancy effects, but in the range of depths studied here, it does not lead to any significant deviations in the cross-stream motion of the droplet [as shown in Fig. 14(b)]. Moreover, the essential physical characteristics remain the same upon changing the depth of the microchannel. Therefore, the effect of the confinement along the depth may be safely neglected in the theoretical model.

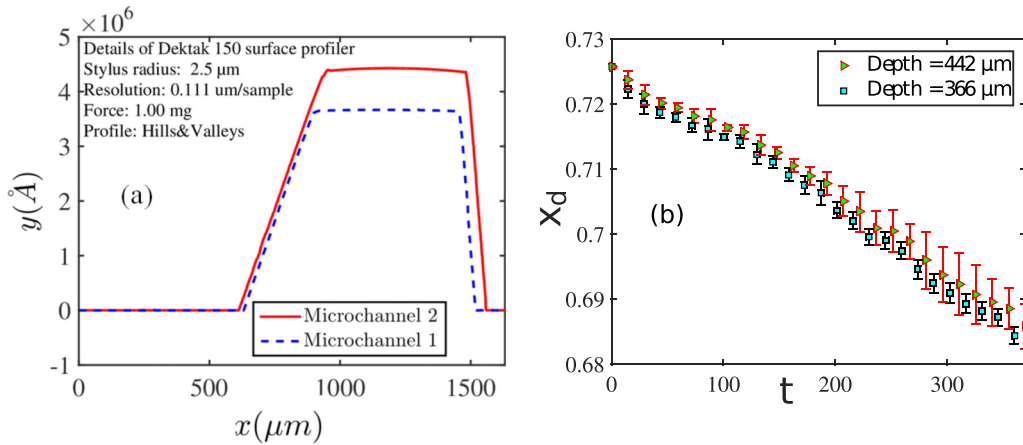


FIG. 14. (a) Measurement of channel depth using Dektak 150 surface profiler. (b) Temporal evolution of droplet centroid in a non-isothermal flow with $Ma_T = 5.5$. The values of the other parameters are taken as $Ma_T = 3.78$, $Bo_d = 2.343$, $Bo_s = 0.2143$, $Wc = 0.35$, and $Re \sim O(10^{-4})$.

-
- [1] H. A. Stone, A. D. Stroock, and A. Ajdari, Engineering flows in small devices: Microfluidics toward a lab-on-a-chip, *Annu. Rev. Fluid Mech.* **36**, 381 (2004).
- [2] C. N. Baroud, F. Gallaire, and R. Dangla, Dynamics of microfluidic droplets, *Lab Chip* **10**, 2032 (2010).
- [3] R. Seemann, M. Brinkmann, T. Pfohl, and S. Herminghaus, Droplet based microfluidics, *Rep. Prog. Phys.* **75**, 016601 (2011).
- [4] D. Di Carlo, D. Irimia, R. G. Tompkins, and M. Toner, Continuous inertial focusing, ordering, and separation of particles in microchannels, *Proc. Natl. Acad. Sci. U.S.A.* **104**, 18892 (2007).
- [5] A. Huebner, S. Sharma, M. Srisa-Art, F. Hollfelder, J. B. Edel, and A. J. Demello, Microdroplets: A sea of applications? *Lab Chip* **8**, 1244 (2008).
- [6] R. Pethig, Dielectrophoresis: An assessment of its potential to aid the research and practice of drug discovery and delivery, *Adv. Drug Delivery Rev.* **65**, 1589 (2013).
- [7] Y. Tao, A. Rotem, H. Zhang, C. B. Chang, A. Basu, A. O. Kolawole, S. A. Koehler, Y. Ren, J. S. Lin, J. M. Pipas *et al.*, Rapid, targeted and culture-free viral infectivity assay in drop-based microfluidics, *Lab Chip* **15**, 3934 (2015).
- [8] Y. Zhu and Q. Fang, Analytical detection techniques for droplet microfluidics: A review, *Anal. Chim. Acta* **787**, 24 (2013).
- [9] S.-Y. Teh, R. Lin, L.-H. Hung, and A. P. Lee, Droplet microfluidics, *Lab Chip* **8**, 198 (2008).
- [10] C. W. Shields IV, C. D. Reyes, and G. P. López, Microfluidic cell sorting: A review of the advances in the separation of cells from debulking to rare cell isolation, *Lab Chip* **15**, 1230 (2015).
- [11] X. C. i Solvas and A. DeMello, Droplet microfluidics: Recent developments and future applications, *Chem. Commun.* **47**, 1936 (2011).
- [12] R. Fåhræus, The suspension stability of the blood, *Physiol. Rev.* **9**, 241 (1929).
- [13] A. Pries, T. W. Secomb, and P. Gaetgens, Biophysical aspects of blood flow in the microvasculature, *Cardiovasc. Res.* **32**, 654 (1996).
- [14] W. Bonner, H. Hulett, R. Sweet, and L. Herzenberg, Fluorescence activated cell sorting, *Rev. Sci. Instrum.* **43**, 404 (1972).
- [15] J. Yang, Y. Huang, X.-B. Wang, F. F. Becker, and P. R. Gascoyne, Cell separation on microfabricated electrodes using dielectrophoretic/gravitational field-flow fractionation, *Anal. Chem.* **71**, 911 (1999).

- [16] G. Hetsroni and S. Haber, The flow in and around a droplet or bubble submerged in an unbound arbitrary velocity field, *Rheol. Acta* **9**, 488 (1970).
- [17] D. P. Panigrahi, S. Das, and S. Chakraborty, Deformation of a surfactant-laden viscoelastic droplet in a uniaxial extensional flow, *Phys. Fluids* **30**, 122108 (2018).
- [18] S. Das, S. Mandal, and S. Chakraborty, Cross-stream migration of a surfactant-laden deformable droplet in a Poiseuille flow, *Phys. Fluids* **29**, 082004 (2017).
- [19] A. Poddar, S. Mandal, A. Bandopadhyay, and S. Chakraborty, Electrical switching of a surfactant coated drop in Poiseuille flow, *J. Fluid Mech.* **870**, 27 (2019).
- [20] S. Mandal, S. Sinha, A. Bandopadhyay, and S. Chakraborty, Drop deformation and emulsion rheology under the combined influence of uniform electric field and linear flow, *J. Fluid Mech.* **841**, 408 (2018).
- [21] N. Behera, S. Mandal, and S. Chakraborty, Electrohydrodynamic settling of drop in uniform electric field: beyond stokes flow regime, *J. Fluid Mech.* **881**, 498 (2019).
- [22] S. Das and S. Chakraborty, Thermally modulated cross-stream migration of a surfactant-laden deformable drop in a Poiseuille flow, *Phys. Rev. Fluids* **3**, 103602 (2018).
- [23] A. J. Griggs, A. Z. Zinchenko, and R. H. Davis, Low-Reynolds-number motion of a deformable drop between two parallel plane walls, *Int. J. Multiphase Flow* **33**, 182 (2007).
- [24] S. Haber and G. Hetsroni, The dynamics of a deformable drop suspended in an unbounded Stokes flow, *J. Fluid Mech.* **49**, 257 (1971).
- [25] S. Mandal, A. Bandopadhyay, and S. Chakraborty, Effect of interfacial slip on the cross-stream migration of a drop in an unbounded Poiseuille flow, *Phys. Rev. E* **92**, 023002 (2015).
- [26] S. Mortazavi and G. Tryggvason, A numerical study of the motion of drops in Poiseuille flow. Part 1. Lateral migration of one drop, *J. Fluid Mech.* **411**, 325 (2000).
- [27] P.-H. Chan and L. Leal, The motion of a deformable drop in a second-order fluid, *J. Fluid Mech.* **92**, 131 (1979).
- [28] A. Karnis, H. Goldsmith, and S. Mason, The flow of suspensions through tubes: V. Inertial effects, *Can. J. Chem. Eng.* **44**, 181 (1966).
- [29] S. C. Hur, N. K. Henderson-MacLennan, E. R. McCabe, and D. Di Carlo, Deformability-based cell classification and enrichment using inertial microfluidics, *Lab Chip* **11**, 912 (2011).
- [30] X. Chen, C. Xue, L. Zhang, G. Hu, X. Jiang, and J. Sun, Inertial migration of deformable droplets in a microchannel, *Phys. Fluids* **26**, 112003 (2014).
- [31] S. Mukherjee and K. Sarkar, Effects of matrix viscoelasticity on the lateral migration of a deformable drop in a wall-bounded shear, *J. Fluid Mech.* **727**, 318 (2013).
- [32] S. Mukherjee and K. Sarkar, Lateral migration of a viscoelastic drop in a Newtonian fluid in a shear flow near a wall, *Phys. Fluids* **26**, 103102 (2014).
- [33] G. Danker, P. M. Vlahovska, and C. Misbah, Vesicles in Poiseuille Flow, *Phys. Rev. Lett.* **102**, 148102 (2009).
- [34] A. Farutin and C. Misbah, Analytical and Numerical Study of Three Main Migration Laws for Vesicles Under Flow, *Phys. Rev. Lett.* **110**, 108104 (2013).
- [35] D. A. Fedosov, M. Peltomäki, and G. Gompper, Deformation and dynamics of red blood cells in flow through cylindrical microchannels, *Soft Matter* **10**, 4258 (2014).
- [36] O. Aouane, M. Thiébaud, A. Benyoussef, C. Wagner, and C. Misbah, Vesicle dynamics in a confined Poiseuille flow: From steady state to chaos, *Phys. Rev. E* **90**, 033011 (2014).
- [37] B. Kaoui, G. Biros, and C. Misbah, Why Do Red Blood Cells Have Asymmetric Shapes Even in a Symmetric Flow? *Phys. Rev. Lett.* **103**, 188101 (2009).
- [38] B. Kaoui, T. Krüger, and J. Harting, How does confinement affect the dynamics of viscous vesicles and red blood cells? *Soft Matter* **8**, 9246 (2012).
- [39] S. Das, S. Mandal, and S. Chakraborty, Effect of temperature gradient on the cross-stream migration of a surfactant-laden droplet in Poiseuille flow, *J. Fluid Mech.* **835**, 170 (2018).
- [40] N. Young, J. S. Goldstein, and M. J. Block, The motion of bubbles in a vertical temperature gradient, *J. Fluid Mech.* **6**, 350 (1959).
- [41] V. Sharanya and G. Raja Sekhar, Thermocapillary migration of a spherical drop in an arbitrary transient Stokes flow, *Phys. Fluids* **27**, 063104 (2015).

- [42] D. Choudhuri and G. Raja Sekhar, Thermocapillary drift on a spherical drop in a viscous fluid, *Phys. Fluids* **25**, 043104 (2013).
- [43] J.-C. Baret, Surfactants in droplet-based microfluidics, *Lab Chip* **12**, 422 (2012).
- [44] L. G. Leal, *Advanced Transport Phenomena: Fluid Mechanics and Convective Transport Processes*, Vol. 7 (Cambridge University Press, Cambridge, 2007).
- [45] J. A. Hanna and P. M. Vlahovska, Surfactant-induced migration of a spherical drop in Stokes flow, *Phys. Fluids* **22**, 013102 (2010).
- [46] O. S. Pak, J. Feng, and H. A. Stone, Viscous Marangoni migration of a drop in a Poiseuille flow at low surface Péclet numbers, *J. Fluid Mech.* **753**, 535 (2014).
- [47] R. W. Flumerfelt, Effects of dynamic interfacial properties on drop deformation and orientation in shear and extensional flow fields, *J. Colloid Interface Sci.* **76**, 330 (1980).
- [48] J. Gounley, G. Boedec, M. Jaeger, and M. Leonetti, Influence of surface viscosity on droplets in shear flow, *J. Fluid Mech.* **791**, 464 (2016).
- [49] A. Ponce-Torres, J. M. Montanero, M. A. Herrada, E. J. Vega, and J. M. Vega, Influence of the Surface Viscosity on the Breakup of a Surfactant-Laden Drop, *Phys. Rev. Lett.* **118**, 024501 (2017).
- [50] S. Das and S. Chakraborty, Influence of complex interfacial rheology on the thermocapillary migration of a surfactant-laden droplet in Poiseuille flow, *Phys. Fluids* **30**, 022103 (2018).
- [51] R. Dangla, S. C. Kayi, and C. N. Baroud, Droplet microfluidics driven by gradients of confinement, *Proc. Natl. Acad. Sci. U.S.A.* **110**, 853 (2013).
- [52] P. Garstecki, H. A. Stone, and G. M. Whitesides, Mechanism for Flow-Rate Controlled Breakup in Confined Geometries: A Route to Monodisperse Emulsions, *Phys. Rev. Lett.* **94**, 164501 (2005).
- [53] H. Wioland, F. G. Woodhouse, J. Dunkel, J. O. Kessler, and R. E. Goldstein, Confinement Stabilizes a Bacterial Suspension into a Spiral Vortex, *Phys. Rev. Lett.* **110**, 268102 (2013).
- [54] D. Wang, M. Hermes, R. Kotni, Y. Wu, N. Tasios, Y. Liu, B. De Nijs, E. B. Van Der Wee, C. B. Murray, M. Dijkstra *et al.*, Interplay between spherical confinement and particle shape on the self-assembly of rounded cubes, *Nat. Commun.* **9**, 2228 (2018).
- [55] H. S. Kim and R. S. Subramanian, Thermocapillary migration of a droplet with insoluble surfactant: I. Surfactant cap, *J. Colloid Interface Sci.* **127**, 417 (1989).
- [56] L. Huang and L.-S. Liu, Simultaneous determination of thermal conductivity and thermal diffusivity of food and agricultural materials using a transient plane-source method, *J. Food Eng.* **95**, 179 (2009).
- [57] M. Nallani and R. S. Subramanian, Migration of methanol drops in a vertical temperature gradient in a silicone oil, *J. Colloid Interface Sci.* **157**, 24 (1993).
- [58] S. Haber and G. Hetsroni, Hydrodynamics of a drop submerged in an unbounded arbitrary velocity field in the presence of surfactants, *Appl. Sci. Res.* **25**, 215 (1972).
- [59] H. Lamb, *Hydrodynamics* (Cambridge University Press, Cambridge, 1993).
- [60] See Supplemental Material at <http://link.aps.org/supplemental/10.1103/PhysRevFluids.6.053603> for expressions of the constant coefficients appearing in Eqs. (22), (30), and (37).
- [61] S. Santra, S. Das, S. S. Das, and S. Chakraborty, Surfactant-induced retardation in lateral migration of droplets in a microfluidic confinement, *Microfluid. Nanofluid.* **22**, 88 (2018).
- [62] S. Santra and S. Chakraborty, Steady axial electric field may lead to controllable cross-stream migration of droplets in confined oscillatory microflows, *J. Fluid Mech.* **907**, A8 (2021).
- [63] C. Kuang, W. Zhao, F. Yang, and G. Wang, Measuring flow velocity distribution in microchannels using molecular tracers, *Microfluid. Nanofluid.* **7**, 509 (2009).